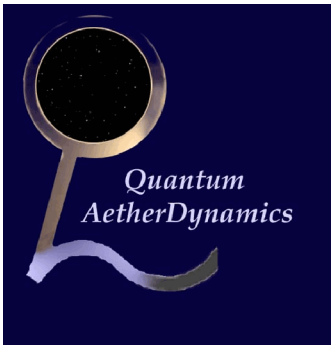

Quantum AetherDynamics Institute (QADI)

Toward QMU Gravitational Field Equations II: Closure-Flow Dynamics, Propagation Waves, and the Newtonian Projection Limit

David W. Thomson III
Quantum AetherDynamics Institute (QADI), Alma, Illinois, USA
ORCID: 0000-0002-5830-5427

Version 1.0 – May 18, 2026

This article is published by the Quantum AetherDynamics Institute (QADI).

It develops the Aether Physics Model (APM)

Abstract

The previous paper established the ontological and geometrical foundations of QMU gravitational structure through rotational propagation density, closure flow, and chronovibrational compression.

The present paper develops the first dynamical field structure arising from the Quantum Measurement Units (QMU) ledger. Rather than treating gravity as passive metric curvature, the framework treats gravity as a closure-flow propagation system within rotational Aether geometry.

A first-order continuity structure is introduced in which closure loading redistributes through allowable propagation geometry. Dynamic propagation-density equations are developed for static, wave-like, and nonlinear closure regimes.

The Newtonian inverse-square law is derived as the low-order SI projection of spherical closure-flow conservation. The rotational torsion operator curl is promoted from a purely mathematical operator to a physical propagation-torsion field quantity governed by Ledger One:

$$A_u \cdot \mathrm{curl} = c^2.$$

The framework naturally permits scalar, longitudinal, torsional, and transverse gravitational propagation modes. Chronovibrational compression is treated as a local propagation-rate coupling to the propagation-density field.

The analysis suggests that conventional gravitational equations are projection relations emerging from deeper closure-flow geometry.

Keywords: QMU, APM, gravitational field equations, closure flow, propagation density, torsion transport, chronovibrational compression, scalar gravitational waves, rotational geometry, Ledger One

1 Introduction

The previous paper established the first-order geometrical interpretation of gravity within the Aether Physics Model (APM). Gravity was interpreted as a propagation-density phenomenon governed by rotational closure geometry rather than passive coordinate curvature. This interpretation differs from conventional metric-curvature approaches originating with Einstein field theory and later tensor formulations Einstein [1916], Misner et al. [1973], Wald [1984].

The central field quantities introduced were:

$$\Phi_g, \qquad J_c, \qquad \rho_{\mathrm{closure}}. \tag{1}$$

The previous work established:

- propagation-density loading,
- closure-flow redistribution,
- chronovibrational compression,
- and propagation-density wave structure.

The present paper develops the next stage of the framework: the first dynamical field equations arising from the QMU ledger.

The objective is not to reproduce general relativity in alternate notation. Instead, the objective is to identify the physically meaningful conservation structures governing rotational propagation geometry.

The new dynamical contributions are closure-flow continuity, propagation-density evolution, torsional transport, nonlinear closure self-interaction, and the Newtonian projection limit.

2 Derivation Strategy

The present paper develops the first dynamical field structure arising from the QMU propagation framework. Because the field program is still at an early stage, it is useful to identify the logical derivation sequence connecting rotational propagation geometry to observable gravitational behavior.

The strategy of the present analysis is therefore to proceed from physically meaningful propagation structures toward their macroscopic SI projections.

The derivation program developed in the following sections consists of seven primary stages.

2.1 Closure-Flow Continuity

The first objective is to establish closure-flow conservation as the primary geometrical conservation law governing propagation redistribution.

Matter imposes closure demand on surrounding propagation geometry. The closure-flow vector:

$$J_c \tag{2}$$

therefore acts as the transport quantity describing redistribution of closure loading through rotational Aether structure.

The continuity equation:

$$\nabla \cdot J_c = \rho_{\text{closure}} \tag{3}$$

becomes the first-order conservation relation of propagation geometry.

2.2 Spherical Closure Redistribution

The second objective is to derive the inverse-square propagation structure from closure-flow conservation across spherical propagation surfaces.

For static spherical systems, closure demand redistributes across the surface:

$$4\pi r^2. \tag{4}$$

The resulting propagation-density field:

$$\Phi_g(r) \propto r^{-2} \tag{5}$$

emerges geometrically from conservation of closure flow rather than from an assumed force law.

2.3 Newtonian Projection Limit

The third objective is to recover the Newtonian gravitational relation as the macroscopic SI projection of closure-flow geometry.

Using the QMU gravitational identity:

$$G = \frac{{\lambda_C}^3 {F_q}^2}{m_a}, \tag{6}$$

the inverse-square propagation-density field projects into the familiar SI form:

$$g(r) = \frac{GM}{r^2}. \tag{7}$$

Newtonian gravity therefore becomes a projection relation emerging from deeper rotational propagation structure.

2.4 Propagation-Density Dynamics

The fourth objective is to develop a dynamical propagation-density equation governing time-dependent closure redistribution.

The first-order field structure:

$$\frac{\partial^2 \Phi_g}{\partial t^2} - v_\Phi^2 \nabla^2 \Phi_g = C \tag{8}$$

introduces propagation-density wave behavior within rotational geometry.

This structure permits scalar, longitudinal, torsional, and transverse closure disturbances.

2.5 Nonlinear Closure Evolution

The fifth objective is to investigate nonlinear propagation effects associated with strong closure loading.

The generalized propagation equation:

$$\frac{\partial^2 \Phi_g}{\partial t^2} - v_\Phi^2 \nabla^2 \Phi_g + \alpha \Phi_g^2 + \beta |\nabla \Phi_g|^2 = C \tag{9}$$

introduces local closure self-interaction and propagation-gradient coupling.

Here, α sets the scale of local closure self-interaction, while β couples gradient steepening to propagation-density evolution.

These nonlinear terms may produce:

- closure-wave steepening,
- trapped harmonic structure,
- nonlinear scattering,
- and closure-boundary resonances.

2.6 Chronovibrational Field Coupling

The sixth objective is to connect propagation-density loading to observable clock-rate variation.

Within the APM framework, clocks operate through physical propagation processes. Local propagation-density compression therefore modifies propagation advancement rates within the present moment.

The resulting chronovibrational coupling relation:

$$F_q' = F_q(1 - \chi_g) \tag{10}$$

provides the first-order connection between gravitational loading and observable frequency variation.

2.7 RMFD Detector Coupling

The seventh objective is to connect propagation-density dynamics to possible experimental observables.

Within RMFD detector systems, longitudinal and torsional propagation-density oscillations may induce correlated magnetic rotational perturbations.

The schematic detector-coupling relation:

$$\mathrm{sclw}_d^* = \frac{1}{F_q}\frac{\partial^2 \xi}{\partial t \partial x} \tag{11}$$

provides the first-order bridge between propagation-density dynamics and experimental scalar-wave detection.

The long-term objective of the derivation program is the development of a fully self-consistent QMU gravitational field theory derived directly from rotational propagation geometry and closure-flow structure.

3 Derivation of the Newtonian Projection from Closure-Flow Conservation

The preceding sections established closure flow as the primary redistribution mechanism governing propagation-density loading within rotational Aether geometry.

The present section develops the first explicit derivation showing how the Newtonian inverse-square law emerges from closure-flow conservation.

The objective is not to assume Newtonian gravity as a primitive force law, but to derive its SI projection structure from conservation of propagation redistribution.

3.1 Spherical Closure Redistribution

Consider a static spherically symmetric closure source with total closure demand associated with mass M.

Let the closure-flow vector be:

$$J_c(\mathbf{r}). \tag{12}$$

For spherical symmetry, the closure flow must be purely radial:

$$J_c(r) = J_r(r)\,\hat{r}. \tag{13}$$

The total closure flux through a spherical propagation surface of radius r becomes:

$$\mathcal{F}_c(r) = \oint J_c \cdot dA. \tag{14}$$

Because the flow is radial and isotropic:

$$\mathcal{F}_c(r) = J_r(r) \oint dA. \tag{15}$$

The spherical surface area is:

$$\oint dA = 4\pi r^2. \tag{16}$$

Therefore:

$$\mathcal{F}_c(r) = 4\pi r^2 J_r(r). \tag{17}$$

This relation represents the total closure redistribution through the surrounding propagation surface.

3.2 Closure-Flow Conservation

Outside the central source region, no additional closure loading is introduced.

The continuity equation therefore reduces to:

$$\nabla \cdot J_c = 0. \tag{18}$$

Thus the total closure flux must remain constant across all surrounding spherical surfaces:

$$\mathcal{F}_c(r) = \text{constant}. \tag{19}$$

Combining with Equation (6) gives:

$$4\pi r^2 J_r(r) = C_M, \tag{20}$$

where C_M represents the total closure demand associated with mass M.

Solving for the radial closure-flow field gives:

$$J_r(r) = \frac{C_M}{4\pi r^2}. \tag{21}$$

The inverse-square structure therefore emerges directly from conservation of closure redistribution through spherical propagation geometry.

No inverse-square force law has been assumed. The resulting inverse-square structure nevertheless reproduces the observable Newtonian projection behavior associated with classical gravitational theory Wheeler [1962].

The geometry alone produces the result.

3.3 Propagation-Density Identification

The propagation-density field Φ_g represents local closure loading within allowable propagation geometry.

To first order, the propagation-density field is proportional to the radial closure redistribution:

$$\Phi_g(r) \propto J_r(r). \tag{22}$$

Substituting Equation (11) gives:

$$\Phi_g(r) \propto \frac{1}{r^2}. \tag{23}$$

The gravitational propagation-density field therefore possesses the same inverse-square structure as the closure-flow geometry from which it emerges.

3.4 Propagation Compression and Acceleration

Within the QMU framework, gravitational acceleration arises from directional propagation compression produced by radial closure flow.

The observable acceleration is proportional to the radial closure-flow field rather than to the derivative of the spherical dilution field:

$$g(r) \propto J_r(r). \tag{24}$$

Since:

$$J_r(r) = \frac{C_M}{4\pi r^2}, \tag{25}$$

the resulting acceleration possesses inverse-square structure:

$$g(r) \propto \frac{1}{r^2}. \tag{26}$$

Spatial gradients in Φ_g govern propagation compression, chronovibrational loading, and local field variation, while the observable Newtonian acceleration follows the radial closure-flow projection.

The Newtonian radial dependence therefore emerges naturally from propagation compression generated by spherical closure-flow conservation.

3.5 QMU Projection Scaling

The QMU gravitational ledger gives:

$$G = \frac{{\lambda_C}^3 {F_q}^2}{m_a}. \tag{27}$$

The numerical SI projection is anchored to the CODATA 2022 recommended fundamental constants Mohr et al. [2025], National Institute of Standards and Technology [2026].

Substituting into the SI gravitational relation:

$$g(r) = \frac{GM}{r^2}, \tag{28}$$

gives:

$$g(r) = \frac{{\lambda_C}^3 {F_q}^2}{m_a} \frac{M}{r^2}. \tag{29}$$

Factoring the natural QMU acceleration scale:

$$\lambda_C {F_q}^2, \tag{30}$$

the acceleration becomes:

$$g(r) = \left(\lambda_C {F_q}^2\right) \left(\frac{M}{m_a}\right) \left(\frac{{\lambda_C}^2}{r^2}\right). \tag{31}$$

This expression shows that gravitational acceleration is fundamentally governed by:

- the QMU acceleration scale $\lambda_C {F_q}^2$,
- the fractional closure demand M/m_a,
- and the spherical propagation dilution factor ${\lambda_C}^2/r^2$.

Newtonian gravity therefore emerges as the low-order SI projection of rotational closure-flow geometry.

3.6 Physical Interpretation

Within the present framework, gravity is not interpreted as an instantaneous force acting across empty space.

Instead:

- matter imposes closure demand,
- closure demand redistributes through propagation geometry,
- propagation density acquires inverse-square structure,
- and free bodies follow the resulting propagation-compression gradient.

The inverse-square law therefore emerges geometrically from conservation of closure redistribution within rotational Aether structure.

The conventional Newtonian gravitational equation becomes the macroscopic SI projection of deeper propagation-flow dynamics.

4 Derivation of the Propagation-Density Wave Equation

The Newtonian projection limit follows from static closure-flow conservation. The next step is to allow the propagation-density field to vary in time.

A time-dependent closure disturbance corresponds to a local compression or relaxation of allowable rotational propagation geometry. Such disturbances must propagate through the surrounding Aether structure rather than appear instantaneously at a distance.

The goal of this section is to derive the first-order wave equation governing small propagation-density disturbances.

4.1 Perturbation of the Propagation-Density Field

Let the propagation-density field be decomposed into a static background and a small dynamical perturbation:

$$\Phi_g(\mathbf{r}, t) = \Phi_0(\mathbf{r}) + \phi(\mathbf{r}, t), \tag{32}$$

where:

- $\Phi_0(\mathbf{r})$ is the static background propagation-density field,
- $\phi(\mathbf{r}, t)$ is the time-dependent closure disturbance.

For weak disturbances:

$$|\phi| \ll |\Phi_0|. \tag{33}$$

The field ϕ represents a local oscillatory compression of propagation density about the background closure state.

4.2 Closure Continuity with Time Dependence

The dynamical closure-flow continuity equation is:

$$\frac{\partial \rho_{\text{closure}}}{\partial t} + \nabla \cdot J_c = S_c. \tag{34}$$

For free propagation outside an active source region:

$$S_c = 0. \tag{35}$$

The continuity equation becomes:

$$\frac{\partial \rho_{\text{closure}}}{\partial t} + \nabla \cdot J_c = 0. \tag{36}$$

To first order, closure-loading density is proportional to the propagation-density disturbance:

$$\rho_{\text{closure}} = \kappa_\rho \phi, \tag{37}$$

where κ_ρ is the closure-loading proportionality factor.

Thus:

$$\kappa_\rho \frac{\partial \phi}{\partial t} + \nabla \cdot J_c = 0. \tag{38}$$

4.3 Closure-Flow Response Law

Closure flow responds to gradients in propagation density. A first-order response law may be written:

$$J_c = -\kappa_J \nabla \psi, \tag{39}$$

where ψ is a propagation displacement potential and κ_J is the closure-flow response coefficient.

The propagation-density disturbance is related to compression of this displacement potential:

$$\phi = -\nabla \cdot \psi. \tag{40}$$

For scalar compression modes, the displacement potential may be treated as a longitudinal field:

$$\psi = \psi_L \hat{n}. \tag{41}$$

The closure-flow response is therefore longitudinal for scalar compression waves.

4.4 Restoring Relation

A compressed propagation-density state produces a restoring response because rotational Aether geometry tends toward closure equilibrium.

The restoring relation is taken in first-order form as:

$$\frac{\partial J_c}{\partial t} = -\kappa_\Phi \nabla \phi, \tag{42}$$

where κ_Φ is the propagation-density restoring coefficient.

Taking the divergence gives:

$$\nabla \cdot \frac{\partial J_c}{\partial t} = -\kappa_\Phi \nabla^2 \phi. \tag{43}$$

Since spatial and temporal derivatives commute:

$$\frac{\partial}{\partial t} (\nabla \cdot J_c) = -\kappa_\Phi \nabla^2 \phi. \tag{44}$$

4.5 Second-Order Field Equation

From the first-order continuity equation:

$$\nabla \cdot J_c = -\kappa_\rho \frac{\partial \phi}{\partial t}. \tag{45}$$

Taking the time derivative:

$$\frac{\partial}{\partial t} (\nabla \cdot J_c) = -\kappa_\rho \frac{\partial^2 \phi}{\partial t^2}. \tag{46}$$

Equating this result with the restoring relation:

$$-\kappa_\rho \frac{\partial^2 \phi}{\partial t^2} = -\kappa_\Phi \nabla^2 \phi. \tag{47}$$

Therefore:

$$\frac{\partial^2 \phi}{\partial t^2} - \frac{\kappa_\Phi}{\kappa_\rho} \nabla^2 \phi = 0. \tag{48}$$

Define the propagation-density wave speed:

$$v_\Phi^2 = \frac{\kappa_\Phi}{\kappa_\rho}. \tag{49}$$

The free propagation-density wave equation becomes:

$$\frac{\partial^2 \phi}{\partial t^2} - v_\Phi^2 \nabla^2 \phi = 0. \tag{50}$$

Restoring the full propagation-density field gives:

$$\frac{\partial^2 \Phi_g}{\partial t^2} - v_\Phi^2 \nabla^2 \Phi_g = C, \tag{51}$$

where C represents source-driven closure loading.

4.6 QMU Propagation-Speed Identification

Ledger One gives the maximum stable propagation-square condition:

$$A_u \cdot \mathrm{curl} = {F_q}^2 {\lambda_C}^2 = c^2. \tag{52}$$

The relation corresponds to the QMU decomposition of the electromagnetic propagation invariant Thomson III [2025a,b].

Since:

$$c = \lambda_C F_q, \tag{53}$$

the natural propagation speed of undisturbed closure-density waves is:

$$v_\Phi \to c = \lambda_C F_q \tag{54}$$

in the weak-loading limit.

Thus the first-order QMU propagation-density wave equation becomes:

$$\frac{\partial^2 \Phi_g}{\partial t^2} - c^2 \nabla^2 \Phi_g = C \tag{55}$$

for weak fields and free propagation geometry.

In strong closure regions, propagation compression may reduce the effective closure-wave speed:

$$v_\Phi < c. \tag{56}$$

4.7 Mode Interpretation

The propagation-density wave equation supports several physically distinct disturbance modes.

For scalar compression modes:

$$\phi = \phi_s. \tag{57}$$

For longitudinal closure oscillations:

$$\phi_L \sim \nabla \cdot \xi, \tag{58}$$

where ξ is longitudinal propagation displacement.

For torsional propagation modes:

$$\phi_T \sim \nabla \times T_r, \tag{59}$$

where T_r is rotational torsion structure.

For transverse rotational shear:

$$\nabla \cdot \phi_\perp = 0. \tag{60}$$

Thus the same propagation-density equation can support scalar, longitudinal, torsional, and transverse gravitational modes depending on the boundary conditions and field geometry.

4.8 Spherical Wave Form

For free spherical propagation outside the source region, the scalar wave equation admits the standard radial form:

$$\phi(r,t) = \frac{A}{r}\cos(kr - \omega t + \delta), \tag{61}$$

where:

- A is wave amplitude,
- k is propagation wavenumber,
- ω is angular frequency,
- and δ is phase offset.

The dispersion relation follows:

$$\omega^2 = v_\Phi^2 k^2. \tag{62}$$

In the weak-loading QMU limit:

$$\omega = ck = \lambda_C F_q k. \tag{63}$$

This shows that the propagation-density disturbance travels at the Ledger One propagation speed in open propagation geometry.

4.9 Physical Interpretation

The wave equation derived above describes oscillatory redistribution of closure loading through rotational propagation geometry.

The derivation shows that propagation-density waves require only:

- closure-flow continuity,
- a restoring response to propagation-density gradients,
- and the QMU propagation-speed condition.

The resulting field equation is:

$$\frac{\partial^2 \Phi_g}{\partial t^2} - v_\Phi^2 \nabla^2 \Phi_g = C. \tag{64}$$

This equation is the dynamical counterpart of the static closure-flow conservation relation.

Static spherical closure redistribution produces the Newtonian projection, while time-dependent closure redistribution produces propagation-density waves.

The framework therefore unifies Newtonian gravitational behavior and scalar gravitational wave behavior as different regimes of the same closure-flow field system.

5 Nonlinear Closure Dynamics

The propagation-density wave equation derived in the previous section describes small disturbances about a weakly loaded background geometry. That linear approximation is appropriate when the propagation-density perturbation remains small compared with the background closure state.

However, strong gravitational systems, horizon boundaries, compact rotating sources, and trapped closure-wave cavities require nonlinear closure dynamics. In these regimes, propagation-density loading modifies the medium through which the disturbance propagates.

The objective of this section is to introduce the first nonlinear extension of the QMU propagation-density field equation.

5.1 Breakdown of the Linear Approximation

The linear propagation-density equation is:

$$\frac{\partial^2 \Phi_g}{\partial t^2} - v_\Phi^2 \nabla^2 \Phi_g = C. \tag{65}$$

This assumes that:

$$|\phi| \ll |\Phi_0|, \tag{66}$$

where:

$$\Phi_g(\mathbf{r}, t) = \Phi_0(\mathbf{r}) + \phi(\mathbf{r}, t). \tag{67}$$

When the disturbance becomes comparable to the background loading:

$$|\phi| \sim |\Phi_0|, \tag{68}$$

the propagation response can no longer be treated as linear.

The field then modifies its own propagation conditions.

This produces nonlinear closure behavior.

5.2 Closure Self-Interaction

Propagation-density loading represents compression of allowable rotational geometry. As this compression increases, additional compression should not remain independent of the existing field state.

The first nonlinear correction is therefore a local closure self-interaction term:

$$\alpha\Phi_g^2. \tag{69}$$

Here, α sets the scale of local closure self-interaction.

This term represents the tendency of strong propagation-density loading to modify the local closure state through its own field amplitude.

A positive α corresponds to increasing resistance against further closure compression. A negative α corresponds to self-focusing or runaway closure concentration.

Thus α controls whether nonlinear closure dynamics are stabilizing or self-amplifying.

5.3 Gradient-Steepening Coupling

Strong closure systems also involve rapidly changing propagation-density gradients.

The first nonlinear gradient correction is:

$$\beta|\nabla\Phi_g|^2. \tag{70}$$

Here, β couples gradient steepening to propagation-density evolution.

This term represents the effect of sharp closure gradients on the local field dynamics.

Regions where:

$$|\nabla\Phi_g| \tag{71}$$

is large may produce:

- closure-wave steepening,
- propagation impedance changes,
- reflection from closure-density boundaries,
- nonlinear scattering,
- and harmonic generation.

Thus β governs how strongly propagation-density gradients affect the evolution of the field.

5.4 First Nonlinear Propagation-Density Equation

Adding the local self-interaction and gradient-steepening terms gives the first nonlinear closure equation:

$$\frac{\partial^2\Phi_g}{\partial t^2} - v_\Phi^2\nabla^2\Phi_g + \alpha\Phi_g^2 + \beta|\nabla\Phi_g|^2 = C. \tag{72}$$

This equation is the first nonlinear extension of QMU propagation-density dynamics.

It contains:

- inertial propagation response,
- spatial propagation redistribution,
- local closure self-interaction,
- gradient-driven closure steepening,
- and source-driven closure loading.

The equation reduces to the linear propagation-density wave equation when:

$$\alpha\Phi_g^2 \to 0, \qquad \beta|\nabla\Phi_g|^2 \to 0. \tag{73}$$

5.5 Effective Propagation-Speed Renormalization

Nonlinear closure loading may also be interpreted as modifying the effective propagation speed of closure disturbances.

Let:

$$v_\Phi = v_\Phi(\Phi_g). \tag{74}$$

For weak nonlinear loading, expand:

$$v_\Phi^2(\Phi_g) = c^2\left(1 - \eta\Phi_g + \cdots\right), \tag{75}$$

where η is a coupling coefficient describing how propagation-density loading reduces effective closure-wave speed.

The nonlinear propagation equation may then be written:

$$\frac{\partial^2\Phi_g}{\partial t^2} - c^2\left(1 - \eta\Phi_g\right)\nabla^2\Phi_g = C. \tag{76}$$

Expanding gives:

$$\frac{\partial^2\Phi_g}{\partial t^2} - c^2\nabla^2\Phi_g + \eta c^2\Phi_g\nabla^2\Phi_g = C. \tag{77}$$

This form shows explicitly how nonlinear closure loading changes the local propagation response of the field.

The coefficient η represents propagation-speed compression caused by local closure loading.

5.6 Closure-Boundary Limit

A closure boundary forms when propagation freedom approaches the limiting closure state.

Let χ_g represent dimensionless closure loading. The open-propagation regime corresponds to:

$$0 \le \chi_g \ll 1. \tag{78}$$

The closure-boundary limit corresponds to:

$$\chi_g \to 1. \tag{79}$$

In this limit, local propagation advancement becomes suppressed:

$$F_q{}' = F_q(1 - \chi_g) \to 0. \tag{80}$$

The effective propagation speed likewise approaches:

$$v_\Phi \to c(1 - \chi_g). \tag{81}$$

Thus:

$$v_\Phi \to 0 \qquad \text{as} \qquad \chi_g \to 1. \tag{82}$$

This identifies the horizon as a closure-locked propagation boundary.

At this boundary, nonlinear terms dominate because propagation-density loading strongly modifies both local field amplitude and gradient response.

5.7 Harmonic Generation

Nonlinear field equations naturally generate harmonic structure.

Suppose the first-order disturbance is:

$$\Phi_g = \Phi_0 + A\cos(kr - \omega t). \tag{83}$$

Then the self-interaction term becomes:

$$\Phi_g^2 = [\Phi_0 + A\cos(kr - \omega t)]^2 \tag{84}$$

$$= \Phi_0^2 + 2\Phi_0 A\cos(kr - \omega t) + A^2\cos^2(kr - \omega t). \tag{85}$$

Using:

$$\cos^2 x = \frac{1}{2}\left(1 + \cos 2x\right), \tag{86}$$

the nonlinear term contains:

$$\cos\left[2(kr - \omega t)\right]. \tag{87}$$

Thus local closure self-interaction generates second harmonic structure.

Higher-order nonlinearities would generate additional harmonics.

This provides a natural mechanism for:

- closure-boundary resonances,
- horizon harmonic modes,
- ringdown-like structures,
- and trapped loxodromic standing waves.

5.8 Propagation Impedance

Nonlinear closure gradients also imply propagation impedance.

Define an effective closure impedance:

$$Z_\Phi \sim \frac{\text{propagation-density pressure}}{\text{closure-flow response}}. \tag{88}$$

A first-order field expression may be written:

$$Z_\Phi \sim \frac{\Phi_g}{|J_c|}. \tag{89}$$

Regions with different propagation-density loading therefore possess different closure impedances.

At a boundary between two closure-density regions:

$$Z_{\Phi,1} \neq Z_{\Phi,2}, \tag{90}$$

propagation-density waves may partially reflect and partially transmit.

This suggests that strong closure gradients can produce:

- wave reflection,
- standing closure modes,
- propagation refraction,
- boundary trapping,
- and nonlinear scattering.

5.9 Physical Interpretation

The nonlinear closure equation:

$$\frac{\partial^2 \Phi_g}{\partial t^2} - v_\Phi^2 \nabla^2 \Phi_g + \alpha \Phi_g^2 + \beta |\nabla \Phi_g|^2 = C \tag{91}$$

describes propagation-density evolution beyond the weak-field approximation.

The coefficient α governs local closure self-interaction.

The coefficient β governs gradient-driven steepening and impedance structure.

The coefficient η governs propagation-speed compression under closure loading.

Together, these nonlinear terms describe how strong gravitational systems may produce:

- closure-wave steepening,
- trapped propagation states,
- harmonic boundary modes,
- nonlinear scalar-wave scattering,
- and horizon closure locking.

The linear wave equation describes open propagation geometry.

The nonlinear equation describes strong closure geometry.

Thus the nonlinear closure dynamics provide the mathematical bridge between weak propagation-density waves and closure-locked horizon behavior.

6 Chronovibrational Field Coupling

The previous sections developed the propagation-density field equations governing closure redistribution and propagation-wave dynamics.

The next step is to connect the propagation-density field to observable physical processes.

Within the Aether Physics Model (APM), clocks are not treated as abstract coordinate devices. Clock behavior emerges from physical propagation processes occurring within rotational Aether geometry.

Atomic oscillations, electromagnetic transitions, resonant phase cycles, and wave propagation all depend upon local propagation advancement rates.

Chronovibrational behavior therefore becomes a direct physical coupling between local propagation-density loading and observable frequency evolution.

6.1 Local Propagation Advancement

The fundamental QMU propagation relation is:

$$c = \lambda_C F_q. \tag{92}$$

Here:

- λ_C represents the quantum propagation length,
- F_q represents the quantum propagation frequency.

Within weak gravitational loading, local propagation advancement proceeds at the open propagation rate:

$$F_q{}' = F_q. \tag{93}$$

However, increasing propagation-density loading compresses allowable rotational propagation geometry.

This compression reduces local phase advancement per cycle.

The local propagation frequency therefore becomes:

$$F_q{}' < F_q. \tag{94}$$

Clock-rate variation is therefore interpreted as altered propagation advancement within the present moment rather than motion among separate time frames.

6.2 Propagation-Density Coupling

The propagation-density field:

$$\Phi_g \sim \frac{\partial \theta}{\partial s} \tag{95}$$

represents local closure loading within rotational geometry.

Increasing Φ_g corresponds to increasing propagation compression.

Define the dimensionless closure-loading parameter:

$$\chi_g = \frac{\Phi_g}{\Phi_{\text{crit}}}, \tag{96}$$

where:

$$0 \leq \chi_g < 1 \tag{97}$$

for open propagation geometry, and:

$$\chi_g \to 1 \tag{98}$$

approaches closure-locking conditions.

The first-order chronovibrational coupling relation becomes:

$$F_q{}' = F_q(1 - \chi_g). \tag{99}$$

This equation states that increasing propagation-density loading suppresses local propagation advancement.

6.3 Frequency Shift

Consider two observers located at differing propagation-density conditions.

Let:

$$F_1 = F_q(1 - \chi_1), \tag{100}$$

and:

$$F_2 = F_q(1 - \chi_2). \tag{101}$$

The observed frequency ratio becomes:

$$\frac{F_2}{F_1} = \frac{1 - \chi_2}{1 - \chi_1}. \tag{102}$$

For weak loading:

$$\chi_g \ll 1, \tag{103}$$

the fractional frequency shift becomes:

$$\frac{\Delta F}{F} \approx -(\chi_2 - \chi_1). \tag{104}$$

Thus gravitational redshift emerges as differential propagation-density loading between two regions of rotational geometry.

6.4 Chronovibrational Compression

The reduction in local propagation advancement produces what may be termed chronovibrational compression.

This compression affects all local physical processes consistently because all local oscillatory systems depend upon the same propagation-density structure.

Thus:

- atomic transitions slow,
- resonant oscillations slow,
- electromagnetic phase cycles slow,
- and local clock rates slow.

The resulting effect is observationally equivalent to relativistic gravitational time dilation while assigning a direct physical propagation mechanism to the phenomenon. Observed gravitational clock-rate shifts and propagation delays have been experimentally verified through photon redshift, airborne atomic-clock measurements, and relativistic satellite synchronization Pound and Rebka [1960], Hafele and Keating [1972], Ashby [2003].

6.5 Propagation Delay

Propagation-density loading also affects the transport of signals through closure geometry.

The effective propagation speed becomes:

$$v_\Phi = c(1 - \chi_g). \tag{105}$$

Regions of increased closure loading therefore produce increased propagation delay.

The propagation time along a path Γ becomes:

$$t_\Gamma = \int_\Gamma \frac{ds}{v_\Phi}. \tag{106}$$

Substituting the chronovibrational propagation relation:

$$t_\Gamma = \frac{1}{c} \int_\Gamma \frac{ds}{1 - \chi_g}. \tag{107}$$

Thus propagation-density loading modifies both local oscillatory rates and signal propagation times.

6.6 Weak-Field Approximation

For weak gravitational loading:

$$\chi_g \ll 1, \tag{108}$$

expand:

$$\frac{1}{1 - \chi_g} \approx 1 + \chi_g. \tag{109}$$

The propagation delay becomes:

$$t_\Gamma \approx \frac{1}{c}\int_\Gamma (1+\chi_g)\,ds. \tag{110}$$

The excess propagation delay is therefore:

$$\Delta t \approx \frac{1}{c}\int_\Gamma \chi_g\,ds. \tag{111}$$

This identifies gravitational propagation delay as the integrated effect of local propagation-density loading along the propagation path.

6.7 Closure-Boundary Limit

As closure loading approaches the limiting propagation state:

$$\chi_g \to 1, \tag{112}$$

local propagation advancement becomes strongly suppressed:

$$F_q{}' \to 0. \tag{113}$$

Likewise:

$$v_\Phi \to 0. \tag{114}$$

The propagation time then diverges:

$$t_\Gamma \to \infty. \tag{115}$$

To distant observers, the closure boundary therefore appears frozen.

Within the present framework, this is not interpreted as motion into another time frame. Instead, the local propagation processes governing physical oscillations become increasingly suppressed by closure loading.

The horizon therefore becomes a chronovibrationally compressed propagation boundary.

6.8 QMU Projection Structure

The chronovibrational coupling relation may be expressed directly in terms of the propagation-density field.

Using:

$$\chi_g = \frac{\Phi_g}{\Phi_{\text{crit}}}, \tag{116}$$

the local propagation frequency becomes:

$$F_q{}' = F_q\left(1-\frac{\Phi_g}{\Phi_{\text{crit}}}\right). \tag{117}$$

Since:

$$\Phi_g \propto \frac{GM}{r^2}, \tag{118}$$

the observable clock-rate variation becomes the SI projection of local propagation-density loading.

Thus relativistic clock behavior emerges naturally from closure-flow geometry.

6.9 Wave-Coupled Chronovibrational Oscillations

Propagation-density waves also produce oscillatory chronovibrational behavior.

Let:

$$\Phi_g(r,t) = \Phi_0(r) + A\cos(kr - \omega t). \tag{119}$$

The local propagation frequency becomes:

$$F_q{}'(r,t) = F_q\left[1 - \frac{\Phi_0(r)}{\Phi_{\text{crit}}} - \frac{A}{\Phi_{\text{crit}}}\cos(kr - \omega t)\right]. \tag{120}$$

Thus scalar gravitational waves produce oscillatory local clock-rate variation.

This provides a direct coupling mechanism between propagation-density waves and precision timing systems.

Potential observable consequences include:

- correlated atomic-clock fluctuations,
- resonant chronovibrational modulation,
- scalar-wave timing signatures,
- and RMFD-coupled oscillatory perturbations.

Related interference and phase-shift behavior associated with rotational and gravitational propagation has previously been observed in neutron and interferometric phase experiments Sagnac [1913], Aharonov and Bohm [1959], Berry [1984], Colella et al. [1975], Bonse and Wroblewski [1983].

6.10 Physical Interpretation

Chronovibrational coupling provides the bridge between propagation-density geometry and observable temporal behavior.

Within the present framework:

- gravity alters propagation density,
- altered propagation density changes local phase advancement,
- altered phase advancement changes observable clock rates,
- and propagation-density waves produce oscillatory timing variations.

The chronovibrational relation:

$$F_q{}' = F_q(1 - \chi_g) \tag{121}$$

therefore acts as the first-order coupling law between propagation geometry and observable temporal phenomena.

Relativistic clock behavior becomes the SI projection of local propagation compression within rotational Aether geometry.

6.11 Half-Spin Matter and Temporal Orientation

Within the APM framework, elementary half-spin matter possesses intrinsic rotational propagation orientation.

The loxodromic propagation structure associated with half-spin particles produces a preferred propagation advancement direction within rotational Aether geometry.

Observed forward temporal behavior therefore emerges from the directional propagation orientation of matter rather than from an independently flowing time dimension.

Chronovibrational compression modifies the local propagation advancement rate, while half-spin rotational structure determines the preferred orientation of that advancement.

The combination of rotational propagation orientation and propagation-density loading produces the observable asymmetry associated with forward temporal evolution.

A complete derivation of temporal orientation from half-spin rotational closure geometry is deferred to future work.

7 Rotational Torsion Transport

In conventional vector calculus, curl is treated as a purely mathematical operator.

Within QMU, however, the torsional quantity becomes physically meaningful.

Ledger One:

$$A_u \cdot \text{curl} = c^2 \tag{122}$$

implies that torsional rotational density is directly tied to allowable propagation structure.

The torsional field quantity may therefore be written:

$$T_r = \text{curl}. \tag{123}$$

Propagation-density transport becomes coupled to torsional transport through:

$$J_c \sim \nabla \times T_r. \tag{124}$$

This relation suggests that closure redistribution occurs through rotational torsion transport within Aether geometry.

The resulting structure resembles a rotational flow system rather than a passive metric geometry.

This torsional interpretation extends the earlier APM torsion program, in which toroidal torsion vacua, holonomy structure, torsion sign reversal, curl thresholds, and electromagnetic transport were developed as physical consequences of Ledger One. The present paper applies that torsion program to gravitational propagation by treating curl not merely as a vector operator, but as the torsional transport structure governing closure-flow redistribution Thomson III [2025c,d,e,f].

8 Experimental Coupling

The framework produces several experimentally testable predictions.

8.1 Scalar Gravitational Modes

Longitudinal propagation-density oscillations should exist.

8.2 RMFD Correlations

Rotational magnetometer systems may detect correlated torsional perturbations.

8.3 Closure Harmonics

Horizons should support trapped rotational harmonic modes.

8.4 Propagation Impedance

Regions of differing propagation density should produce:

- wave reflection,
- standing modes,
- propagation refraction,
- and closure scattering.

9 Toward Tensor Reconstruction

Within QMU, conventional gravitational equations are interpreted as projection relations emerging from deeper propagation geometry.

The metric tensor may therefore represent an SI projection operator describing:

- closure-flow redistribution,
- propagation compression,
- and chronovibrational loading.

The framework suggests that:

$$g_{\mu\nu} \tag{125}$$

is not fundamentally primitive, but rather an emergent geometrical projection of deeper rotational propagation structure as in conventional relativistic formulations Einstein [1916], Misner et al. [1973], Wald [1984].

10 Limitations and Future Development

The present analysis establishes only the first-order dynamical structure of the QMU gravitational field program. A complete theory will require covariant closure-transport equations, tensor reconstruction operators, self-consistent source coupling, nonlinear horizon solutions, and quantitative comparison with precision timing, gravitational-wave, and astrophysical observations.

11 Conclusion

A first-order dynamical gravitational field structure has been developed from closure-flow conservation and rotational propagation geometry.

The framework treats gravity as a closure-flow propagation system rather than passive coordinate curvature.

The primary field quantities are:

$$\Phi_g, \qquad J_c, \qquad \rho_{\text{closure}}, \qquad T_r, \qquad \chi_g. \tag{126}$$

Newtonian gravity emerges as the SI projection of spherical closure-flow conservation. The inverse-square structure follows from redistribution of closure demand through spherical propagation surfaces, while the QMU projection scaling gives:

$$g(r) = \left(\lambda_C {F_q}^2\right)\left(\frac{M}{m_a}\right)\left(\frac{{\lambda_C}^2}{r^2}\right). \tag{127}$$

Time-dependent closure redistribution produces the propagation-density wave equation:

$$\frac{\partial^2 \Phi_g}{\partial t^2} - v_\Phi^2 \nabla^2 \Phi_g = C. \tag{128}$$

Nonlinear closure dynamics introduce local closure self-interaction, gradient-steepening behavior, propagation-speed compression, harmonic generation, and closure-boundary impedance.

Chronovibrational field coupling connects propagation-density loading to observable clock-rate variation through:

$${F_q}' = F_q(1 - \chi_g). \tag{129}$$

Rotational torsion transport connects the field equations to the broader APM torsion program by treating curl as a physical torsional transport structure governed by Ledger One.

The analysis suggests that conventional gravitational theory may represent the projection layer of a deeper rotational closure geometry governed by the QMU ledger. The broader QADI torsion, closure, and propagation program is developed across the archived institute papers and conversion references Thomson III [2025g, 2026].

Acknowledgments

The Quantum AetherDynamics Institute (QADI) is a private 501(c)(3) research institute developing the Aether Physics Model (APM) and Quantum Measurement Units (QMU) Thomson III [2025g]. Publications and data are archived with DOIs in the AetherPhysics Zenodo community: zenodo.org/communities/aetherphysics.

References

Albert Einstein. Die Grundlage der allgemeinen Relativitätstheorie. *Annalen der Physik*, 354(7): 769–822, 1916. doi: 10.1002/andp.19163540702.

Charles W. Misner, Kip S. Thorne, and John Archibald Wheeler. *Gravitation*. W. H. Freeman and Company, San Francisco, 1973. ISBN 9780716703440.

Robert M. Wald. *General Relativity*. University of Chicago Press, Chicago, 1984. ISBN 9780226870335.

John Archibald Wheeler. *Geometrodynamics*. Academic Press, New York, 1962.

Peter J. Mohr, David B. Newell, Barry N. Taylor, and Eite Tiesinga. Codata recommended values of the fundamental physical constants: 2022. *Reviews of Modern Physics*, 97(2):025002, 2025. doi: 10.1103/RevModPhys.97.025002. URL https://link.aps.org/doi/10.1103/RevModPhys.97.025002.

National Institute of Standards and Technology. The nist reference on constants, units, and uncertainty. https://physics.nist.gov/cuu/Constants/, 2026. Accessed: 2026-05-18.

David W. Thomson III. Reference tables for quantum measurement unit (qmu) conversions: Cgs and mks systems, November 2025a. URL https://doi.org/10.5281/zenodo.17683574.

David W. Thomson III. The charge conversion factor in the aether physics model: From singular to distributed charge, with rules, exceptions, and benchmarks, October 2025b. URL https://doi.org/10.5281/zenodo.17451188.

R. V. Pound and G. A. Rebka. Apparent weight of photons. *Physical Review Letters*, 4(7):337–341, 1960. doi: 10.1103/PhysRevLett.4.337.

J. C. Hafele and Richard E. Keating. Around-the-world atomic clocks: Predicted relativistic time gains. *Science*, 177(4044):166–168, 1972. doi: 10.1126/science.177.4044.166.

Neil Ashby. Relativity in the global positioning system. *Living Reviews in Relativity*, 6(1), 2003. doi: 10.12942/lrr-2003-1.

Georges Sagnac. L'ether lumineux demontre par l'effet du vent relatif d'ether dans un interferometre en rotation uniforme. *Comptes Rendus de l'Academie des Sciences*, 157:708–710, 1913.

Yakir Aharonov and David Bohm. Significance of electromagnetic potentials in the quantum theory. *Physical Review*, 115(3):485–491, 1959. doi: 10.1103/PhysRev.115.485.

M. V. Berry. Quantal phase factors accompanying adiabatic changes. *Proceedings of the Royal Society of London. Series A*, 392(1802):45–57, 1984. doi: 10.1098/rspa.1984.0023.

R. Colella, A. W. Overhauser, and S. A. Werner. Observation of gravitationally induced quantum interference. *Physical Review Letters*, 34(23):1472–1474, 1975. doi: 10.1103/PhysRevLett.34.1472.

U. Bonse and T. Wroblewski. Measurement of neutron quantum interference in noninertial frames. *Physical Review Letters*, 51(16):1401–1404, 1983. doi: 10.1103/PhysRevLett.51.1401.

David W. Thomson III. The josephson effect and rotational closure transport, 2025c. URL https://zenodo.org/records/17451847.

David W. Thomson III. Golden ratio torsion vacua and rotational closure geometry in the aether physics model, 2025d. URL https://zenodo.org/records/18023337.

David W. Thomson III. Gravity control locally via curl thresholds, 2025e. URL https://zenodo.org/records/17544759.

David W. Thomson III. Geometric foundations of particle masses, 2025f. URL https://zenodo.org/records/17267029.

David W. Thomson III. Quantum aetherdynamics institute (qadi): Community doi overview and citation guide. Zenodo, 2025g. URL https://doi.org/10.5281/zenodo.17479314.

David W. Thomson III. Quantum aetherdynamics institute research papers. https://quantumaetherdynamics.org/papers, 2026. Accessed: 2026-05-18.